Curvature sorting of proteins on a cylindrical lipid membrane tether connected to a reservoir

Pankaj Singh, Paritosh Mahata, Tobias Baumgart, and Sovan Lal Das

Phys. Rev. E **85**, 051906 — Published 14 May 2012

DOI: 10.1103/PhysRevE.85.051906

Curvature sorting of proteins on a cylindrical lipid membrane tether connected to a lipid reservoir

Pankaj Singh and Paritosh Mahata
Department of Mechanical Engineering, Indian Institute of Technology, Kanpur 208016, India

Tobias Baumgart
Department of Chemistry, University of Pennsylvania, Philadelphia, USA

Sovan Lal Das*
Department of Mechanical Engineering, IIT Kanpur, Kanpur 208016, India

Membrane curvature of a biological cell is actively involved in various fundamental cell biological functions. It has been discovered that membrane curvature and binding of peripheral membrane proteins follow a symbiotic relationship. The exact mechanism behind this interplay of protein binding and membrane curvature has not yet been properly understood. To elucidate the mechanism, we study curvature sorting of proteins in a model system of a tether pulled from a Giant Unilamellar Vesicle (GUV) using mechanical-thermodynamic models. The concentration of proteins bound to membrane changes significantly due to curvature. This has also been observed in experiments by other researchers. We also find that there is a phase transition based on protein concentration and we discuss co-existence of phases and stability of solutions. Furthermore, when sorting is favorable, the increase in protein concentration stabilizes the tether in the sense that less pulling force is required to maintain the tether. A similar mechanism may be in place, when motor proteins pull tethers from donor membranes.

PACS numbers: 87.16.D-, 82.70.Uv, 87.10.-e
Keywords: curvature sorting, curvature sensing, membrane protein, lipid bilayer

* Corresponding author; sovandas@iitk.ac.in

I. INTRODUCTION

Membrane curvature is no longer considered a passive geometric feature of biological cell membrane. It plays an active role in the fundamental cell biological processes by controlling the spatial organization [1–3]. Proteins play equally important role in these activities. One of the key aspect for many of these cellular functions is the membrane curvature sensing and generation (MC-S&G) through the binding of peripheral membrane proteins [1].

The mechanisms of MC-S&G have been classified into four main categories based on their distinct qualitative features. They are briefly mentioned below. More details can be found in literature, eg., [1, 4]. Using the *scaffolding* mechanism proteins with intrinsic curvature locally concentrate to induce curvature within the membrane[3]. Depending on the type of proteins involved, this mechanism leads to cylindrical or spherical curvature [3, 5–7]. A second mechanism is *hydrophobic insertion*. In this mechanism, the proteins involved insert their hydrophobic domains into membrane bilayer (wedging) to generate curvature [8]. The inserting domains are either helical [9–11] or non-helical [12–14]. Certain proteins individually can not bend/sense membranes significantly. However, due to the cooperative effect these proteins *oligomerize* into a lattice-like coats. Using this polymerization mechanism proteins can amplify MC-S&G [6, 15–19]. It has also been observed that many proteins involved in MC-S&G lack intrinsic curvature (hence no scaffolding), hydrophobic inserting domains or tendency to cooperatively aggregate (i.e oligomerize). Such proteins may induce curvature via *local crowding* [4, 20, 21].

Researchers have identified and classified proteins that are involved in MC-S&G based on their structures. The first family of proteins contain a BAR (Bin/Amphiphysin/RVs) domain. BAR domains are crescent-shaped $\alpha-$helical bundles. They bind to membrane mainly via hydrophobic insertion mechanism or electrostatic interaction, and use scaffolding mechanism while interacting with membrane curvature. The second family of proteins, the dynamin family of proteins [22], also interact with membrane curvature using scaffolding mechanism, however, do not contain a BAR domain. The third class involves proteins that do not use scaffolding mechanism based on their structure. They use the inserting mechanism to generate curvature. Typically, these proteins have intrinsically unfolded structure. Upon binding to membrane they undergo folding transition to form amphipathic $\alpha-$helices.

Most theoretical studies on protein binding are concerned with adsorption on flat lipid bilayer. Chatelier and Minton [23] modeled proteins as regular convex hard particles and predicted that the cooperativity among proteins (tendency of self association) influences the protein adsorption isotherm and it deviates from the Langmuir isotherm (for adsorption of ideal gases). Later Minton [24, 25] extended the study by incorporating different protein conformations, effect of area inclusion, and clustering via a kinetic model. Zhdanov and Kasemo [26], using a chemical kinetics model for protein adsorption and desorption, predicted an existence of a critical protein coverage fraction above which adsorption is negatively affected. Heimburg et al. [27] developed a model and conducted experiments for peripheral protein binding on a DOPG/DOPC bilayer. The model takes into account the long-range electrostatic interaction among proteins, along with an equation of state for protein distribution, and a statistical thermodynamics model for lipid distribution in the bilayer while predicting the binding isotherms.

Studies involving the curvature sorting and binding of proteins in giant unilamellar vesicles (GUVs) has been gaining attention in recent times. Raynwar et al. [28] conducted coarse grained molecular simulations that show that the curvature inducing proteins get absorbed on lipid bilayer experience attractive interaction due to curvature. Sorre and coworkers [18, 29], in their experimental investigation, observed that proteins, apart from sensing and generating

curvature, also facilitate and amplify lipid segregation near phase separation point. Furthermore, the nature of MC-S&G depends on protein concentration. Curvature sorting of lipids and its influence on the bending stiffness of the bilayer membrane was studied by Tian et al. [19, 30]. In the dynamic sorting of lipids and proteins, studied by Heinrich et al.[31], nucleation of disordered membrane domains have been observed to occur at the junction between the tether and the GUV. Incidentally, solution of membrane shape equations obtained from bending elasticity model, shows that the curvature is highest at the junction. Capraro et al. [32] investigated the curvature sensing of protein epsin with N-terminal homology (ENTH) and derived the spontaneous curvature of ENTH/PIP2 complex. It was also noted that ENTH binds preferentially to membranes with large curvature.

In this contribution, we investigate curvature sorting of proteins in a tether pulled from a GUV using mechanical-thermodynamic models. We employ Helfrich model for bending elasticity of the membrane with membrane spontaneous curvature proportional to protein concentration, and Van der Waals or Bragg-Williams models with interaction for the proteins binding to membrane. We first discuss sorting on a catenoid-like shape and, subsequently, sorting on a cylindrical tube. We observe that, except for the neck region of the catenoid the two scenarios are almost identical. We discuss sorting in a tube in detail including, the phase transition based on protein concentration, co-existence of phases and stability of solutions. Finally, we fit model predictions to recent experimental data, obtained from Refs. [29, 33], and estimate various parameters including the intrinsic curvature of proteins.

II. CURVATURE SORTING IN A CATENOID

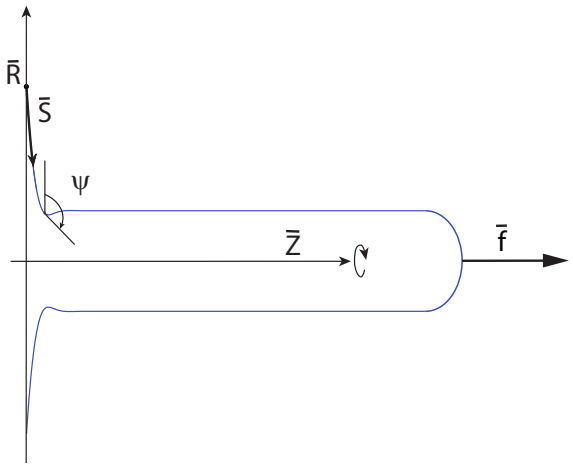

FIG. 1. (Color online) Schematic of a catenoid along with the definition of geometric variables.

We consider a situation when a tube (tether) is connected to a membrane reservoir (GUV). Typically a tether has diameters in the range of 20-100nm, whereas the diameter of a GUV is 5μm or more. Accordingly, we can consider this to be a tether pulled from a flat membrane. In such a case the shape of the tether is that of a catenoid as shown in figure 1. In the following we derive the shape equations of the catenoid in the scenario when proteins bind to the outer surface. The free energy has contributions from the bending elasticity of the bilayer membrane [34], the mixing

free energy of proteins modeled as a gas [18], and a spontaneous curvature linear in protein concentration [29]. An equivalent model exists where a term that couples composition and curvature linearly is included in the free energy [1, 35]. Free energy of the catenoid is then given by

$$\bar{F} = 2\pi \int \bar{\mathcal{L}} dt \,, \tag{1}$$

where the Lagrangian $\bar{\mathcal{L}}$ with mixing free energy is

$$\bar{\mathcal{L}} = \left[\frac{\kappa}{2} \left(\frac{\psi'}{\bar{S}'} + \frac{\sin\psi}{\bar{R}} - \bar{C}_0 \right)^2 + \bar{\Sigma} + \frac{\bar{P}\bar{R}}{2} \sin\psi + \bar{\Gamma}(\theta) \right] \bar{R}\bar{S}' + \bar{\gamma}(\bar{R}' - \bar{S}'\cos\psi) - \frac{\bar{f}}{2\pi}\bar{S}'\sin\psi \,.$$

Here, t is a generalized parameter, $\bar{S}$ is arclength, ψ is the tangent angle at any point on the catenoid measured from vertical, $\bar{R}$ is the radial distance from the axis of symmetry, $\bar{\Sigma}$ is the lateral tension in the membrane, κ is the bending stiffness of the membrane, $\bar{C}_0$ is the spontaneous curvature of the membrane, $\bar{P}$ is the pressure across the membrane, prime ($\prime$) denotes derivatives with respect to t. Pulling force $\bar{f}$ is required to maintain a stable length of the tether and $\bar{\gamma}$ is a Lagrange multiplier for the geometric constraint [36]. We consider that the membrane spontaneous curvature is linear in protein concentration, i.e., $\bar{C}_0 = \theta \bar{C}_p$, where $\bar{C}_p$ is the intrinsic curvature of protein molecules and we assume that it does not depend on membrane curvature. The function $\bar{\Gamma}(\theta)$, where θ is the coverage fraction of proteins, is Legendre transformed free energy density (due to mixing only) of the proteins [37]:

$$\bar{\Gamma}(\theta) = \bar{f}_m(\theta) - \frac{\bar{\mu}_{ves}\theta}{\bar{b}} + \bar{\Pi}_{ves} \,,$$

where $\bar{f}_m$ is the free energy (per unit area) of the proteins due to mixing and protein-protein interaction, $\bar{b}$ is the area occupied by an individual molecule, $\bar{\mu}_{ves}$ is the chemical potential of the proteins bound to the vesicle (the lipid reservoir), and $\bar{\Pi}_{ves}$ is the fixed pressure of the proteins on the vesicle. Note that $\bar{\mu}_{ves}$ is also fixed and is equal to the chemical potential of the proteins in the aqueous solution. Note that $\bar{\Gamma}(\theta_{ves}) = 0$, when $\bar{C}_p = 0$.

Before proceeding further we non-dimensionalize the quantities as follows. Lengths are made dimensionless by a reference tube radius R_0, energy is made dimensionless by the bending rigidity κ, and forces are made dimensionless by the ratio of κ and R_0. That is

$$F = \frac{\bar{F}}{\kappa} \,, \quad S = \frac{\bar{S}}{R_0} \,, \quad R = \frac{\bar{R}}{R_0} \,, \quad C_0 = \bar{C}_p R_0 \,, \quad \gamma = \frac{\bar{\gamma} R_0}{\kappa} \,, \quad f = \frac{\bar{f} R_0}{\kappa} \,, \quad \Sigma = \frac{\bar{\Sigma} R_0^2}{\kappa} \,, \quad \Gamma = \frac{\bar{\Gamma} R_0^2}{\kappa} \,.$$

With this the dimensionless free energy and the Lagrangian are

$$F = 2\pi \int \mathcal{L} dt \,, \tag{2}$$

$$\mathcal{L} = \left[\frac{1}{2} \left(\frac{\psi'}{S'} + \frac{\sin\psi}{R} \right)^2 - C_0\,\theta \left(\frac{\psi'}{S'} + \frac{\sin\psi}{R} \right) + \Sigma + \frac{PR}{2}\sin\psi + \Gamma(\theta) + \frac{C_0^2\theta^2}{2} \right] RS' + \gamma(R' - S'\cos\psi) - \frac{f}{2\pi} S'\sin\psi \,. \tag{3}$$

The Euler-Lagrange equations that determine the shape of the catenoid are given by

$$\frac{\partial \mathcal{L}}{\partial q} - \frac{d}{dt}\left(\frac{\partial \mathcal{L}}{\partial q'} \right) = 0 \,,$$

where q takes up values of ψ, R, θ, and S. The explicit equations are given by

$$\ddot{\psi} = \frac{\sin\psi\,\cos\psi}{R^2} - \frac{\cos\psi\dot{\psi}}{R} + \left(1 + \frac{C_0^2}{\alpha} \right) \left(\frac{PR}{2}\cos\psi + \frac{\gamma}{R}\sin\psi - \frac{f}{2\pi R}\cos\psi \right) \,. \tag{4}$$

$$\dot{\gamma} = \left(\dot{\psi}^2 - \frac{\sin^2\psi}{R^2}\right) - C_0\theta\left(\dot{\psi} - \frac{\sin\psi}{R}\right) + \frac{PR}{2}\sin\psi + \frac{\gamma}{R}\cos\psi + \frac{f}{2\pi R}\sin\psi\,. \tag{5}$$

$$\dot{\theta} = \frac{C_0}{\alpha}\left(\frac{PR}{2}\cos\psi + \frac{\gamma}{R}\sin\psi - \frac{f}{2\pi R}\cos\psi\right)\,. \tag{6}$$

In the above

$$\alpha = \Gamma''(\theta) = f_m''(\theta)\,,$$

and the overdot denotes derivative with respect to the dimensionless arclength S. Equation (6) is obtained by differentiating the Euler-Lagrange equation corresponding to θ

$$-C_0\left(\dot{\psi} + \frac{\sin\psi}{R}\right) + \Gamma'(\theta) + C_0^2\theta = 0\,, \tag{7}$$

and using equation (4) for $\ddot{\psi}$ in the resulting expression. Equation (7) also provides a relation for the dependence of composition on curvature.

The differential equations for R and Z in axisymmetric scenario are

$$\dot{R} = \cos\psi \quad \text{and} \quad \dot{Z} = \sin\psi\,. \tag{8}$$

From the Euler-Lagrange equation for S and the corresponding boundary condition that $\partial\mathcal{L}/\partial S' = 0$ we have the Hamiltonian

$$\mathcal{H} \equiv \partial\mathcal{L}/\partial S' = R\left[\frac{1}{2}\left(\dot{\psi}^2 - \frac{\sin^2\psi}{R^2}\right) - \Sigma - \Gamma(\theta) - \frac{C_0^2\theta^2}{2}\right] + C_0\theta\sin\psi - \frac{PR^2}{2}\sin\psi + \gamma\cos\psi + \frac{f}{2\pi}\sin\psi = 0\,.$$

The boundary conditions obtained from variational principle are

$$\left[\dot{\psi} + \frac{\sin\psi}{R} - C_0\theta\right]_{S=0} = 0\,, \quad \gamma(S_{end}) = 0\,, \tag{9}$$

and

$$\Sigma = \left[\frac{1}{2}\left(\dot{\psi}^2 - \frac{\sin^2\psi}{R^2}\right) - \Gamma(\theta) + C_0\theta\frac{\sin\psi}{R} - \frac{PR}{2}\sin\psi + \frac{\gamma}{R}\cos\psi + \frac{f}{2\pi R}\sin\psi - \frac{C_0^2\theta^2}{2}\right]_{S=0}\,. \tag{10}$$

Other boundary conditions are

$$\theta(0) = \theta_{ves}\,, \quad Z(0) = 0\,, \quad \psi(S_{end}) = \frac{\pi}{2}\,, \tag{11}$$

and when the catenoid area is fixed the condition

$$Z(S_{end}) = L_{tube}\,,$$

L_{tube} being the specified catenoid length, is imposed to compute the pulling force f.

III. CURVATURE SORTING OF PROTEINS USING VAN DER WAALS MODEL

The mixing and interaction energy of the proteins per unit membrane area, when they are modeled as Van der Waals gas, is given by

$$\bar{f}_m(\theta) = -\frac{k_BT}{\bar{b}}\theta\ln\left(\frac{1-\theta}{\theta}\right) - \frac{k_BT}{\bar{b}}\theta - \bar{a}\frac{\theta^2}{\bar{b}^2}\,,$$

where T is absolute temperature, k_B is the Boltzmann's constant, and $\bar{a}$ is a measure of the strength of protein-protein interactions. When made dimensionless $\bar{b}$ and $\bar{a}$ become

$$b = \frac{\kappa}{k_B T}\frac{\bar{b}}{R_0^2} \quad \text{and} \quad a = \frac{\bar{a}}{(k_B T)^2}\frac{\kappa}{R_0^2}\,.$$

With this, the dimensionless f_m is

$$f_m(\theta) = -\frac{1}{b}\theta \ln\left(\frac{1-\theta}{\theta}\right) - \frac{\theta}{b} - a\frac{\theta^2}{b^2}\,, \tag{12}$$

and if the proteins bound to the vesicle membrane are also modeled as Van der Waals gas, then the dimensionless μ_{ves} and Π_{ves} are

$$\mu_{ves} = -\ln\left(\frac{1-\theta_{ves}}{\theta_{ves}}\right) - \frac{\theta_{ves}}{1-\theta_{ves}} - 2a\frac{\theta_{ves}}{b} - \frac{C_0\, b}{R_{ves}} + bC_0^2\theta_{ves} \quad \text{and} \quad \Pi_{ves} = \frac{1}{b}\frac{\theta_{ves}}{1-\theta_{ves}} - a\frac{\theta_{ves}^2}{b^2} + \frac{C_0^2\theta_{ves}^2}{2}\,, \tag{13}$$

where θ_{ves} is the (fixed) protein coverage fraction on the vesicle membrane. Vesicle radius is much larger than the tether radius and we consider $1/R_{ves} = 0$ in subsequent calculations. Finally, Γ in the dimensionless form is

$$\Gamma(\theta) = f_m(\theta) - \frac{\mu_{ves}\theta}{b} + \Pi_{ves}\,.$$

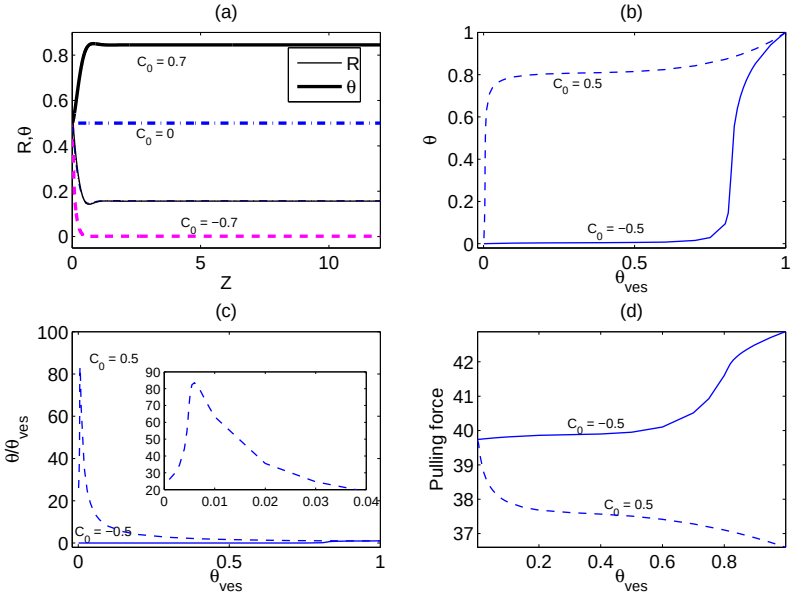

FIG. 2. (Color online) Numerical solution of the shape equations for Van der Waals mixing energy with $a = 3$, $b = 1$, $\Sigma = 20$, $L_{tube} = 12$ and C_0 as shown. (a) The shape (thin- solid, dashed, and dash-dot lines) and the variation protein concentration (thick- solid, dashed, and dash-dot lines) along the length for $\theta_{ves} = 0.5$. The catenoid shapes for different values of C_0 do not differ significantly from each other. The variations (b) $\theta(S_{end})$ with θ_{ves}; (c) normalized $\theta(S_{end})$ with θ_{ves} (an enlarged view for small θ_{ves} has been shown in inset); and (d) pulling force f with θ_{ves}.

We numerically integrate the shape equations (4) through (6) and (8) along with the boundary conditions (9) through (11), with f_m, μ_{ves} and Π_{ves} as given by equations (12) and (13), respectively. The catenoid shape and the variation of protein coverage fraction θ and pulling force f obtained from numerical solution, for a set of parameter

values, are shown in figure 2. Note that the quantities such as protein coverage fraction and curvature vary significantly in the region where shape/curvature changes rapidly. We observe from figure 2(a) that for positive C_0 proteins sort favourably into the tube portion (higher curvature), the reverse happens for negative C_0, and curvature has no influence on sorting when C_0 is zero. In figures 2(b) and 2(c) we present the variation of tube protein coverage fraction and the same normalized by vesicle protein concentration. Figure 2(b) shows that for negative C_0 protein concentration on the tube is always less than that on the vesicle membrane, and up to a significantly large θ_{ves} protein concentration remains low on the tube. Beyond $\theta_{ves} \approx 0.8$ protein concentration on the tube experiences a rapid increase, however, it is still below θ_{ves}. The rapid increase is due to crowding of proteins on the vesicle at higher concentration. The increase of θ with θ_{ves} also correlates with the increase of pulling force with θ_{ves} (figure 2(d)). For positive C_0 sorting effect is much more significant. For $\theta_{ves} \approx 0.0055$, the protein concentration on the tube is approximately 85 times of θ_{ves}. For θ_{ves} less than 0.04, the normalized tube protein coverage fraction is higher than 20. Such a large increase in protein density has also been observed experimentally [29, 33, 38]. Around $\theta_{ves} \approx 0.05$ saturation in tube protein coverage fraction has been observed. This is again due to crowding effect on the tube. Also, note that in this case increase of θ with θ_{ves} also correlates with the decrease in pulling force (figure 2(d)). This implies that protein binding increases the stability of the tether, in the sense that less force is required to maintain the tube at specified length. Similar mechanism may be in place, when motor proteins pull tethers from donor membranes such as Golgi network, and peripheral protein binding helps maintaining such tubular regions [39, 40].

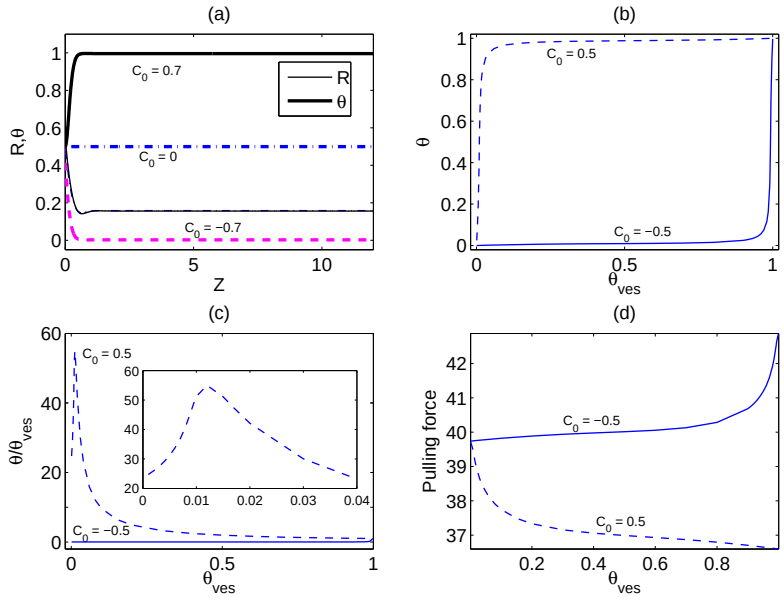

FIG. 3. (Color online) Numerical solution of the shape equations for Bragg-Williams mixing energy with $\chi = 1.5$, $b = 1$, $\Sigma = 20$, $L_{tube} = 12$ and C_0 as shown. (a) The shape (thin- solid, dashed, and dash-dot lines) and the variation protein concentration (thick- solid, dashed, and dash-dot lines) along the length for $\theta_{ves} = 0.5$. The catenoid shapes for different values of C_0 do not differ significantly from each other. The variations (b) $\theta(S_{end})$ with θ_{ves}; (c) normalized $\theta(S_{end})$ with θ_{ves} (an enlarged view for small θ_{ves} has been shown in inset); and (d) pulling force f with θ_{ves}.

IV. CURVATURE SORTING OF PROTEINS USING BRAGG-WILLIAMS MODEL

We now model proteins using Bragg-Williams mean field theory. The mixing and interaction energy of the proteins (dimensionless form) in this case is given by

$$f_m(\theta) = \frac{1}{b}[\theta \ln\theta + (1-\theta)\ln(1-\theta) + \chi\theta(1-\theta)]\,, \tag{14}$$

where the last term corresponds to protein-protein interactions. The quantities μ_{ves} and Π_{ves} are

$$\mu_{ves} = \ln\left(\frac{\theta_{ves}}{1-\theta_{ves}}\right) + \chi(1-2\theta_{ves}) - \frac{C_0 b}{R_{ves}} + bC_0^2\theta_{ves} \quad \text{and} \quad \Pi_{ves} = -\frac{1}{b}[\ln(1-\theta_{ves}) + \chi\theta_{ves}^2] + \frac{C_0^2\theta_{ves}^2}{2}\,. \tag{15}$$

Numerical solutions of the shape equations (4) through (6) and (8) along with the boundary conditions (9) through (11), with f_m, μ_{ves} and Π_{ves} energy as given by equations (14) and (15), respectively, are presented in figure 3. Parameter values, except the molecular interaction parameter χ, are same as those considered for the Van der Waals model. Behavior of the solutions in this case has been qualitatively the same as that observed for Van der Waals gas model presented in figure 2. However, in this case sorting effect is somewhat less significant. In the cylindrical region these quantities are almost constant. Furthermore, from figures 2a and 3a we can conclude that protein coverage fraction has been significantly influenced by the sign of C_0, however, the catenoid shape remains almost the same.

We finally note that the values of a or χ, b, and C_0 are chosen such that the proteins remain in the unique stable configuration. They do not satisfy the condition for dynamic curvature-instability observed by Leibler [41]. The parameter regime in which multiple stable state are observed has not been considered for the catenoid. This regime will be considered for the sorting on a cylinder. This scenario facilitates analytical or semi-analytical determination of stability and coexistence of solutions. Accordingly, in the following we describe the curvature dependent sorting in a cylinder, enabling us to derive conditions for stability and coexistence of solutions analytically.

V. CURVATURE SORTING ON A CYLINDER

The form of the free energy, in the dimensionless form, for a cylinder is (for $P = 0$)

$$F = 2\pi RL\left[\frac{1}{2R^2} - \frac{C_0\theta}{R} + \Sigma + \frac{C_0^2\theta^2}{2} + \Gamma(\theta)\right] - fL\,,$$

where L is the dimensionless length of the cylinder of radius R. The term fL is the work done on the tube by externally applied pulling force. For equilibrium the derivatives of the free energy with respect to R, θ, and L should be zero, which give

$$\mu_{ves} = \mu_{tube} = b\,f_m'(\theta) - \frac{C_0 b}{R} + C_0^2 b\,\theta\,, \quad \Sigma = \frac{1}{2R^2} - \Gamma(\theta) - \frac{C_0^2\theta^2}{2}\,, \quad \text{and} \quad \frac{f}{2\pi} = \frac{1}{R} - C_0\theta\,. \tag{16}$$

To obtain a solution for θ with other parameters fixed, we combine the first two equations of (16) to eliminate R and solve the resulting equation using a root finding technique. We compare the solutions of the cylinder with the solutions of the catenoid shape equations. We present the comparison between the catenoid and cylinder solutions for protein concentration and pulling force for both Van der Waals gas and Bragg-Williams models for an exemplary set of parameter values in figure 4. We find extremely good agreements between the cylinder and catenoid solutions for these and other quantities such as, R and variation of θ with respect to Σ (not shown). Accordingly, in the following we investigate curvature sorting on a cylinder, which gives equations that are analytically tractable.

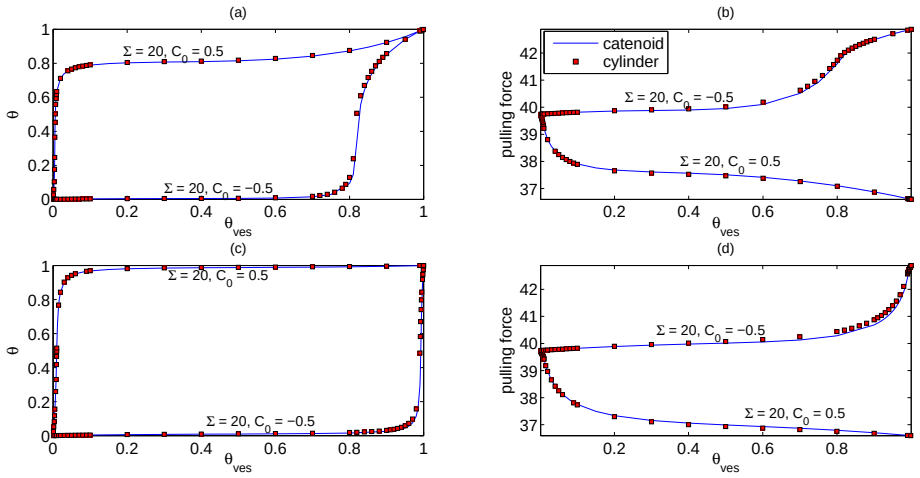

FIG. 4. (Color online) Comparison of some quantities obtained from numerical solution of the catenoid shape equations and the algebraic equations for the cylinder with $b = 1$ and $L_{tube} = 12$. (a) Tube protein concentration and (b) pulling force vs θ_{ves} for the Van der Waals gas model for $a = 3$. (c) Tube protein concentration and (b) pulling force vs θ_{ves} for the Bragg-Williams model for $\chi = 1.5$. Other parameter values are as mentioned in the plots.

In figure 5, we present the variation of protein coverage fraction normalized by vesicle protein coverage fraction with $1/\sqrt{\Sigma}$ for $\theta_{ves} = 0.1$ and 0.05. Note, from second of equation (16), that for $\theta = \theta_{ves}$, initial tube radius R is inversely proportional to $\sqrt{\Sigma}$. So, the results suggest that the normalized protein coverage fraction increases sharply (about 16 fold or higher for $\theta_{ves} = 0.05$) with decrease in tube radius. The increase in tube protein coverage fraction is even larger for smaller values of θ_{ves} as observed in figures 2 and 3. Similar sorting effect has been observed for N-BAR domains on liposomes in a SLiC assay by Bhatia and coworkers [38]. There the authors claim that sensing is due to N-terminal helices and defects on the liposome surface. In our study, the effect of helices and BAR domain curvature has been accounted for by assuming that the spontaneous curvature is the product of protein concentration and the intrinsic curvature of individual BAR domain. However, a comparison between our study and the experimental results of Ref. [38] is not possible as the experimental conditions are different because the tube/catenoid is connected to the lipid reservoir and the mechanisms of sorting may be different [1]. The packing defects have not been explicitly considered in our simple model.

We know that both Van der Waals or Bragg-Williams mixing model exhibit first order phase transition. It has been shown in [33] that the curvature composition coupling model using Van der Waals type mixing predicts such phase transition. Condition for stability is

$$\left(\frac{\partial^2 F}{\partial R^2}\right)\left(\frac{\partial^2 F}{\partial \theta^2}\right) - \left(\frac{\partial^2 F}{\partial R \partial \theta}\right)^2 > 0\,, \quad \text{or} \quad f''_m(\theta) > 0\,.$$

For the Van der Waals and the Bragg-Williams models the condition is explicitly given by

$$\frac{a}{b} \leq \frac{1}{2\theta(1-\theta)^2} \quad \text{and} \quad \chi \leq \frac{1}{2\theta(1-\theta)}\,, \tag{17}$$

respectively. The critical values of a and χ are,

$$\frac{a_{crit}}{b} = \frac{27}{8} \;\; (\text{for } \theta = \frac{1}{3}) \quad \text{and} \quad \chi_{crit} = 2 \;\; (\text{for } \theta = \frac{1}{2})\,. \tag{18}$$

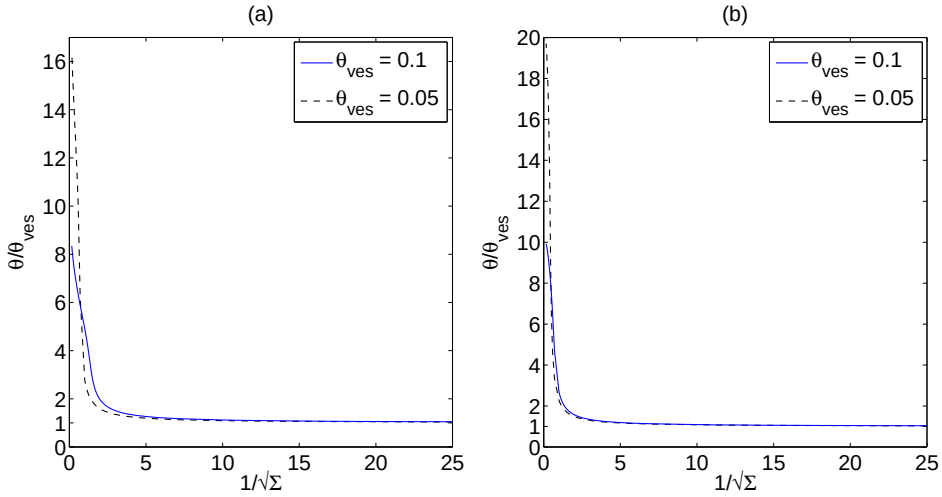

FIG. 5. (Color online) Normalized tube protein concentration vs $1/\sqrt{\Sigma}$ or the initial tube radius for the Van der Waals (left) and Bragg-Williams (right) models. For small initial tube radius we observe a large increase in protein density in the tube.

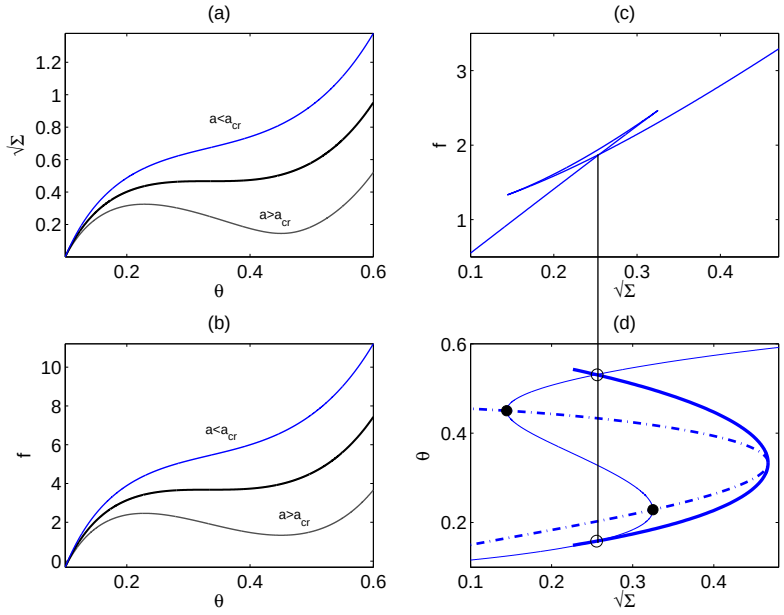

FIG. 6. (Color online) (a) and (b): Variation of $\sqrt{\Sigma}$ and pulling force f, respectively, with protein coverage fraction for the Van der Waals interaction parameters a above and below the critical value. (c) Pulling force with $\sqrt{\Sigma}$ for a above a_{crit}. A Gibbs loop is seen and the self-intersection corresponds to the values of f and Σ at coexistence. (d) The binodal (thick solid) and spinodal (dash-dot) curves in $\theta - \sqrt{\Sigma}$ plane. The points on the binodal are obtained by finding the outermost intersections (marked by open circles) of the vertical line from the coexistence point in (c) with the θ vs $\sqrt{\Sigma}$ (thin solid) curve. The points on the spinodal corresponds to the turning points (filled circles) of the θ vs $\sqrt{\Sigma}$ curve.

Using Eq. (16), we compute variation of lateral tension Σ and pulling force f with θ for different values of a above and below a_{crit} (for Van der Waals gas model). Such variations are shown in figures 6 (a) and (b), respectively. Note that for a range of θ below θ_{ves} pulling force and/or Σ become negative (not shown). Such values of θ are not

considered as a physically feasible solution. For $a < a_{crit}$, for a given Σ, there is a unique θ, which is also the stable solution. For $a > a_{crit}$, there exist multiple solutions (multiple values of θ), for a specified Σ, out of which the solution with intermediate θ is unstable and the other two are locally stable. Multiple equilibrium solutions already satisfy the condition of same chemical potential (first of Eq. (16)). In this case we have a mechanical condition for co-existence that the pulling force, given by last of Eq. (16), must be the same for the coexisting solutions, that is,

$$f(\theta_1, \Sigma) = f(\theta_2, \Sigma)\,. \tag{19}$$

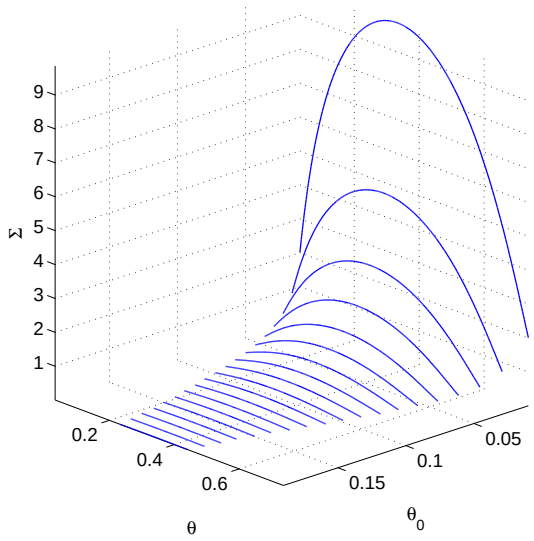

FIG. 7. (Color online) Coexistence curve for Van der Waals model for different θ_{ves} for $b = 1$. Ranges of values of θ and Σ become narrower with increasing θ_{ves}.

Note also that the pulling force is the free energy of the tube per unit length, whose variation with $\sqrt{\Sigma}$ has been shown in figure 6(c). Existence of a Gibbs loop indicates that the system undergoes a first order phase transition and the point of self-intersection provides the values for f and Σ at coexistence [37]. The corresponding values of θ are the outer most intersections with $\sqrt{\Sigma} - \theta$ curve, as shown in figure 6(d). The spinodal obtained from the first of Eq. (17) has also been shown. We mention that the binodal and spinodal curves change with the parameter values chosen. In particular, with increasing θ_{ves} the range of θ values in which solutions coexist become narrower as shown in figure 7. Cryoelectron microscopy studies of lipid vesicles exposed to endophilin have shown existence of coated tubules of different morphologies reflecting the local protein concentration [17]. The observations can be considered as a possibility for the existence of a first order phase transition and coexistence of solutions predicted in our study.

VI. COMPARISON WITH EXPERIMENTS

We now fit our model predictions to the experimental report on curvature sorting, of endophilin N-BAR domain, presented in figures 2E and 2F of [33] for two different solution concentrations of proteins. Fitting results from [33], the

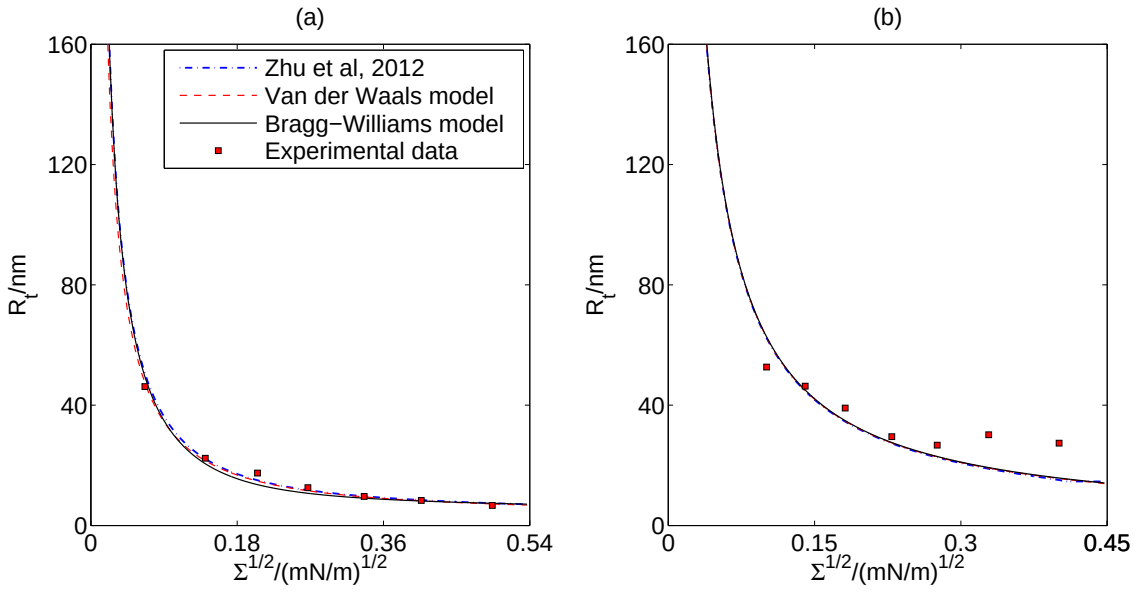

FIG. 8. (Color online) Comparison of model prediction with experimental results. Best fit curves to experimental data of figs. (a) 2E and (b) 2F of Zhu et al. [33] for the Van der Waals and the Bragg-Williams models. Fitted parameter values are shown in table I.

Van der Waals model, and the Bragg-Williams model, respectively, have been shown in figure 8 and the corresponding best fit values have been presented in table I. The fitted values of the parameters are close to each other for all the scenarios. Small differences between our fitted values using the Van der Waals model and those reported in [33] have been observed. One likely reason for such differences is that Zhu et al. [33] fitted simultaneously to protein sorting as well as tube curvature measurements, whereas here we fit to sorting measurements only. Note also that the Bragg-Williams model predicts a smaller spontaneous curvature. Furthermore, for 40nM solution concentration this models predicts the excluded area of proteins to be 0.27nm^2 which is much smaller than the value of 50nm^2-53nm^2 obtained via cryoelectron microscopy reconstruction [17].

We also fit our model to the experimental data for the sorting of protein amphiphysin 1 obtained from figures 2A (force vs. $\sqrt{\Sigma}$), 2B (radius vs. $\sqrt{\Sigma}$) and 2C (sorting vs. radius) of Sorre et al. [29] as shown in figure 9. We conduct a two parameter fit to estimate C_0 and a or χ. The values of $\bar{b}$ and θ_{ves} were taken to be 50nm^2 and $280/\mu m^2$, respectively [29]. The corresponding best fit values have been provided in table II. We find that our model fits experimental data well. Except in figure 9(b) the Van der Waals and Bragg-Williams models differ significantly. The values of spontaneous curvature for the Van der Waals model and Bragg-Williams model are close to each other. Furthermore, Sorre et al. [29] obtained the intrinsic curvatures of the proteins as $\bar{C}_p^{-1} = 1.9nm$ (or $\bar{C}_p = 0.526nm^{-1}$), by fitting a linear model without interaction to their data given in figure 2C. From table II, we find that this agrees with our fitted values of $\bar{C}_p = 0.531nm^{-1}$ (Van der Waals) or $\bar{C}_p = 0.533nm^{-1}$ (Bragg-Williams) and zero magnitude of the interaction parameter. We also note that the fitted values of the interaction parameter a figure 8(b) and χ in figure 9(a) are above their critical values given by Eq. (18). Once again, this indicates the possibility of coexistence of solutions with different protein concentrations which has not been observed in experiments so far. However, further experimental investigation is needed to observe and characterize such coexistence of solutions.

Solution concentration	Parameters	Van der Waals ([33])	Van der Waals (present)	Bragg-Willliams (present)
(a) 1μM (fig 2E of [33])	C_0	139.94 (0.14 nm^{-1})	168.81 (0.17 nm^{-1})	118.26 (0.12 nm^{-1})
	b	0.0011 (56.54 nm^2)	0.00078 (40.10 nm^2)	0.00083 (42.66 nm^2)
	θ_{ves}	0.096	0.1429	0.1454
	a	0.00024 (12.34 $k_BT$nm^2)	0.00017 (8.74 $k_BT$nm^2)	–
	χ	–	–	0.7522 (0.7522 k_BT)
(b) 40nM (fig 2F of [33])	C_0	18.94 (0.019 nm^{-1})	18.94 (0.019 nm^{-1})	5.83 (0.006 nm^{-1})
	b	0.0013 (66.83 nm^2)	0.00076 (39.06 nm^2)	0.0000052 (0.27 nm^2)
	θ_{ves}	0.019	0.0189	0.0083
	a	0.0045 (231.32 $k_BT$nm^2)	0.0038 (195.34 $k_BT$nm^2)	–
	χ	–	–	0.2077 (0.2077 k_bT)

TABLE I. (Color online) Best fit parameter values corresponding to figure 8. Corresponding dimensional values are mentioned within parentheses. Dimensional values are obtained using the scaling radius $R_0 = 1\mu$m and bending stiffness $\kappa = 0.8 \times 10^{-19}$ J.

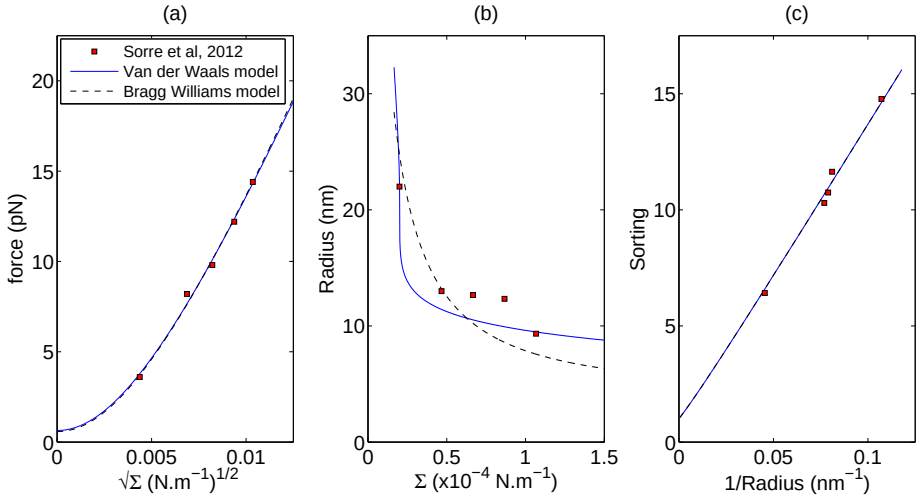

FIG. 9. (Color online) Comparison of model prediction with experimental results. Best fit curves to experimental data of figs. (a) 2A, (b) 2B and (c) 2C of Sorre et al. [29], respectively, for the Van der Waals and the Bragg-Williams models. Fitted parameter values are shown in table II.

VII. CONCLUSION

In this study, we discuss curvature sorting of proteins on a catenoid pulled from a vesicle and cylinder using a mixing free energy for the proteins and Helfrich bending energy for the bilayer membrane. We first find that on the catenoid the quantities vary a little on the cylindrical region. We subsequently, discuss sorting on a cylinder of uniform radius. A comparison with the catenoid model show that the cylinder model approximates the catenoid very well. For varying protein concentration on the vesicle, we find that with positive protein intrinsic curvature there is a large increase (maximum 65-90 fold) increase in tube protein coverage fraction. Furthermore, with increasing initial tube radius, quantified by the vesicle lateral tension, and the vesicle protein concentration the tube protein concentration decay.

Experimental Data	Parameters	Van der Waals	Bragg-Willliams
(a) Fig. 2A of [29]	C_0	42.8903 (0.043 nm^{-1})	34.6521 (0.035 nm^{-1})
	a	0.005909 (295.45 k_BTnm^2)	–
	χ	–	4.31897 (4.31897 k_bT)
(b) Fig. 2B of [29]	C_0	106.0896 (0.106 nm^{-1})	170.6186 (0.171 nm^{-1})
	a	0.0033781 (168.91 k_BTnm^2)	–
	χ	–	0 (0 k_bT)
(c) Fig. 2C of [29]	C_0	530.7457 (0.531 nm^{-1})	533.1961 (0.533 nm^{-1})
	a	0 (0 k_BTnm^2)	–
	χ	–	0 (0 k_BT)

TABLE II. Best fit parameter values corresponding to figure 9. Corresponding dimensional values are mentioned within parentheses. Dimensional values are obtained using the scaling radius $R_0 = 1\mu$m and bending stiffness $\kappa = 20k_BT$. The values $\bar{b} = 50nm^2$ and $\theta_{ves} = 280/\mu m^2$ are taken from Ref. [29].

This is an indication of curvature sensing by proteins and subsequent sorting. Such sorting of endophilin N-BAR and amphiphysin N-BAR domains have been observed experimentally in liposomes. However, exact mechanisms of sorting in liposome and the tether connected to a reservoir may be different. Such differences will be considered in detail in future. We compare our model prediction with the two different sets of recent experimental data and obtained good agreement in most cases. In a few cases, the fitted value of the interaction parameters are higher than the critical values indicating the possibility of first order phase transition in experiments. This has so far not been observed. We also investigate a first order phase transition and coexistence of solutions in our model. Further experimental study is needed to characterize such coexistence of solutions.

ACKNOWLEDGMENTS

TB acknowledges funding from NIH grant R01 GM097552 and NSF grant MCB-0718569. SLD would like to thank IITK for support through grant INT/IITK/ME/20090343.

[1] T. Baumgart, B. Capraro, C. Zhu, and S. L. Das, Annu. Rev. Phys. Chem **62**, 483 (2011).

[2] J. Zimmerberg and S. McLaughlin, Current Biology **14**, R250 (2004).

[3] J. Zimmerberg and M. M. Kozlov, Nat. Rev. Mol. Cell. Biol. **7**, 9 (2006).

[4] H. T. McMahon and J. L. Gallop, Nature **438**, 590 (2005).

[5] A. Frost, R. Perera, A. Roux, K. Spasov, O. Destaing, E. Egelman, P. de Camilli, and V. M. Unger, Cell **132**, 807 (2008).

[6] B. J. Peter, H. M. Kent, I. G. Mills, Y. Vallis, P. Jonathan, G. Butler, P. R. Evans, and H. T. McMahon, Science **303**, 495 (2004).

[7] K. Farsad and P. D. Camilli, Current Opinion in Cell Bilogy **15**, 372 (2003).

[8] F. Campelo, H. T. McMahon, and M. M. Kozlov, Biophys. J. **95**, 2325 (2008).

[9] M. G. J. Ford, I. G. Mills, B. J. Peter, Y. Vallis, and et al., Nature **419**, 361 (2002).

[10] T. Itoh, S. Koshiba, T. Kigawa, A. Kikuchi, S. Yokoyama, and T. Takenawa, Science **291**, 1047 (2001).

[11] Y. Yoon, J. S. Tong, P. J. Lee, A. Albanese, and N. B. et al., Journal of the Biological Chemistry **285**, 531 (2010).

[12] S. Martens, M. M. Kozlov, and H. T. McMahon, Science **316**, 1205 (2007).

[13] X. Cao, U. Coskun, M. Rössle, S. B. Buschhorn, and et al., PNAS **106**, 21121 (2009).

[14] Q. Wang, M. V. Navarro, G. Peng, and et al., PNAS **106**, 12700 (2009).

[15] K. Takei, V. I. Slepnev, V. Haucke, and P. D. Camilli, Nature Cell Biology **1**, 33 (1999).

[16] K. Farsad, N. Ringstad, K. Takei, K. Rose, and P. D. Camilli, Journal of Cell Bilogy **155**, 193 (2001).

[17] N. Mizuno, C. C. Jao, R. Langen, and A. C. Steven, Journal of the Biological Chemistry **285**, 23351 (2010).

[18] B. Sorre, A. Callan-Jones, J.-B. Manneville, P. Nassoy, J.-F. Joanny, J. Frost, B. Goud, and P. Bassereau, PNAS **106**, 5622 (2009).

[19] A. Tian, B. R. Capraro, C. Esposito, and T. Baumgart, Biophys. J. **97**, 1636 (2009).

[20] P. Sens and M. S. Turner, Biophys. J. **86**, 2049 (2004).

[21] J. C. Stachowiak, C. C. Hayden, and D. Y. Sasaki, PNAS **107**, 7781 (2010).

[22] G. J. K. Praefcke and H. T. McMahon, Nat. Rev. Mol. Cell Biol. **5**, 133 (2005).

[23] R. C. Chatelier and A. P. Minton, Biophys. J **71**, 2367 (1996).

[24] A. P. Minton, Biophys. J **76**, 176 (1999).

[25] A. P. Minton, Biophys. J **80**, 1641 (2001).

[26] V. P. Zhdanov and B. Kasemo, Biophys. Chemistry **146**, 60 (2010).

[27] T. Heimburg, B. Angerstein, and D. Marsh, Biophys. J. **76**, 2575 (1999).

[28] B. J. Reynwar, G. Illya, V. A. Harmandris, M. M. Müller, and M. Deserno, Nature **464**, 461 (2007).

[29] B. Sorre, A. Callan-Jones, J. Manzi, and et al, PNAS **109**, 173 (2012).

[30] A. Tian and T. Baumgart, Biophys. J. **96**, 2676 (2009).

[31] M. Heinrich, A. Tian, C. Esposito, and T. Baumgart, PNAS **107**, 7208 (2010).

[32] B. R. Capraro, Y. Yoon, W. Cho, and T. Baumgart, JACS **132**, 1200 (2010).

[33] C. Zhu, S. L. Das, and T. Baumgart, Biophysical Journal **102**, 1837 (2012).

[34] W. Helfrich, Z. Naturforsch **28c**, 693 (1973).

[35] S. Leibler, in *Statistical mechanics of membranes and surfaces*, edited by D. Nelson, T. Piran, and S. Weinberg (Springer-Verlag, Berlin, Germany, 2004).

[36] F. Jülicher and R. Lipowsky, Physical Review E **53**, 2670 (1996).

[37] H. B. Callen, *Thermodynamics and Introduction to Thermostatistics*, 2nd ed. (John Wiley & Sons, NY, 1985).

[38] V. K. Bhatia, K. L. Madsen, P. Y. Bolinger, and et al, The EMBO Journal **28**, 3303 (2009).

[39] S. L. Dabora and M. P. Sheetz, Cell **54**, 27 (1988).

[40] Y. Shibata, J. Hu, M. K. Kozlov, and T. A. Rapoport, Annu. Rev. Cell Dev. Biol. **25**, 329 (2009).

[41] S. Leibler, Journal of Physics (France) **47**, 507 (1986).